LASER INTERFEROMETER GRAVITATIONAL WAVE OBSERVATORY
- LIGO -
CALIFORNIA INSTITUTE OF TECHNOLOGY
MASSACHUSETTS INSTITUTE OF TECHNOLOGY

Document Type **LIGO-T010023-00 - R** 03/01/01

The Thermal Noise Interferometer: First Test Cavity Lock

Eric Black, Seiji Kawamura, Luca Matone, Shanti Rao and Kevin Schultz

Distribution of this draft:

This is an internal working note
of the LIGO Project..

California Institute of Technology
LIGO Project - MS 51-33
Pasadena CA 91125
Phone (626) 395-2129
Fax (626) 304-9834
E-mail: info@ligo.caltech.edu

Massachusetts Institute of Technology
LIGO Project - MS 20B-145
Cambridge, MA 01239
Phone (617) 253-4824
Fax (617) 253-7014
E-mail: info@ligo.mit.edu

WWW: http://www.ligo.caltech.edu/

1 INTRODUCTION

The objective of the Thermal Noise Interferometer (TNI) is to measure and understand one of LIGO's limiting noise sources: the thermal noise of suspended mirrors. The experimental setup will ultimately consist of a laser system shining light onto two suspended Fabry-Perot cavities. An interferometric measurement would then allow to infer the displacement sensitivity of the instrument due to thermal noise once the other noise sources are reduced.

The aim of this report is to describe the state of the TNI at the time of the writing of this document. The instrument has been characterized, various control topologies have been investigated and a variety of noise sources have been studied. The instrument's displacement sensitivity curve will be given, reaching the 10^-15 m/rHz level at 1kHz limited by laser frequency noise.

2 SETUP AND OBJECTIVE

The experimental setup (figure 1) consists of a laser system (Lightwave NPRO 126), a reference cavity consisting of a cylindrical fused silica spacer with mirrors optically contacted to each end, and a suspended Fabry-Perot cavity of 1cm in length and a designed Finesse of 10^5. Difficulties, probably attributed to the laser source, were encountered in locking the suspended Mode-Cleaner. For this reason, the triangular cavity was bypassed and the beam was sent directly to the test cavity. The optical configuration here under study consists of the laser and the suspended test cavity, where the reference cavity served as a diagnostic tool.

The investigations were directed in two steps. First, the laser was locked to the reference cavity thus allowing to

1. quantify the laser PZT driver efficiency
2. estimate the free running laser frequency noise and
3. test the home made amplifiers for the operation of the modecleaner.

Once the characterization of the laser and the test of the electronics was completed, we proceeded in locking the suspended test cavity. In this case, we

1. quantified the transfer function describing
   - the modulation/demodulation process,the optical and photodiode response;
   - the mirror actuator frequency response;
2. explored different control topologies, all of which consisting in actuating on the laser PZT driver and the mirror actuator;
3. locked the test cavity with the use of the home made electronics (designed to operate the suspended Mode Cleaner);
4. estimated the interferometer displacement sensitivity, quantified different noise sources and pinpoint the limiting noise source.

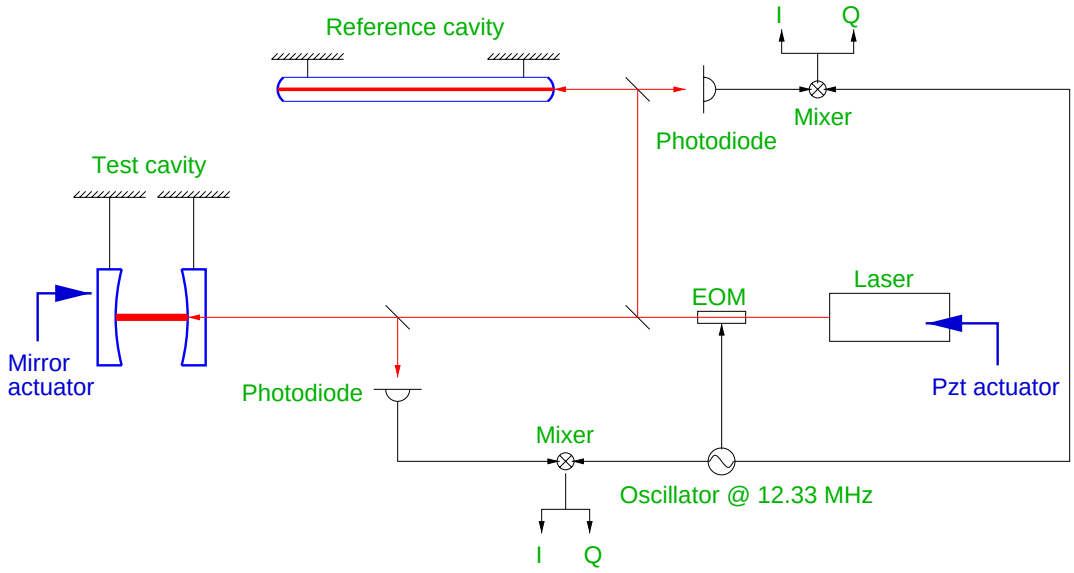

Figure 1: The block diagram representation of the experimental apparatus. By acting on the laser's PZT driver, we studied the laser's performance with respect to the reference. In a separate experiment, by acting on both the laser's PZT driver and one of the test cavity mirror actuator, we were able to lock the laser to the test cavity at high frequency and to lock the test cavity to the laser at low frequencies.

3 FREE RUNNING LASER FREQUENCY NOISE

The reference cavity consists of a cylindrical fused silica spacer with mirrors optically contacted to each end, isolated from vibrations by suspending it with two short wire loops and enclosed in a vacuum vessel. In the high frequency regime, we assume that the cavity length perturbations are smaller than laser frequency noise. Therefore, by locking the laser to the reference, the error and control signals would give an estimate on the free running laser frequency noise. The setup of the measurement is shown in figure 2.

The reference cavity is often used as the first stage of a frequency stabilization system, thus defining the laser frequency of the laser. With the aid of the block diagram shown in figure 2, the residual frequency noise $\delta\nu_{res}$ is related to the free running frequency noise $\delta\nu$ by

$$\frac{\delta\nu_{res}}{\delta\nu} = \frac{1}{1 + C \times H \times P}$$

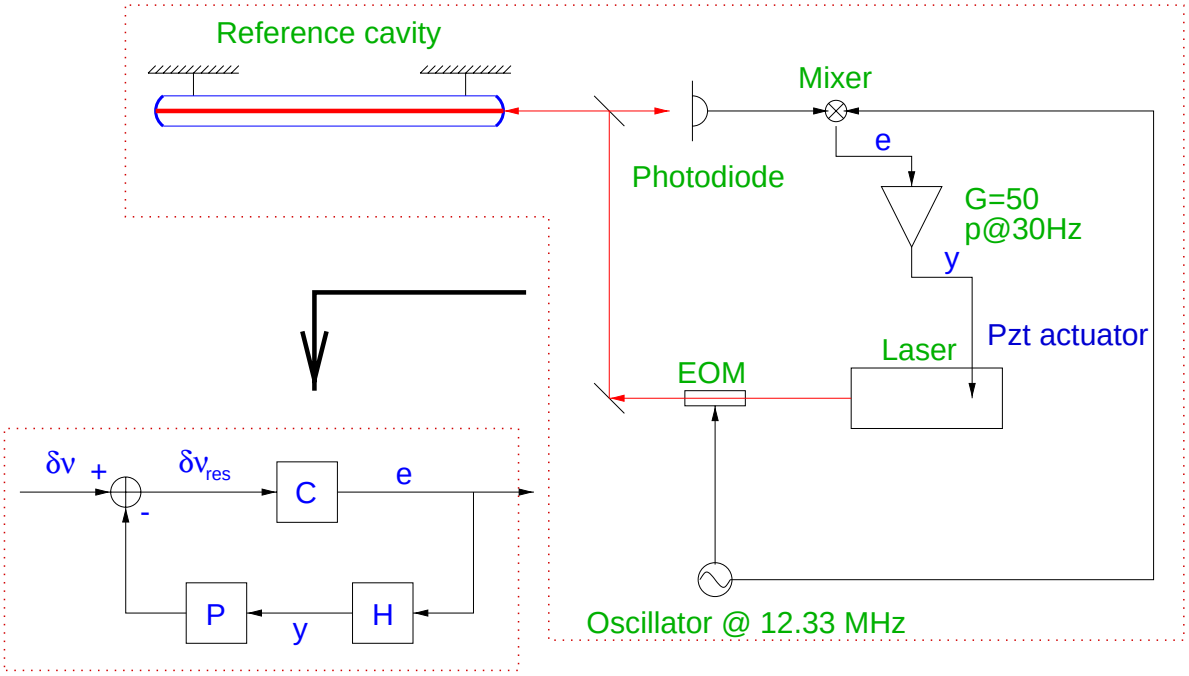

Figure 2: The experimental setup for the free running laser frequency noise. The equivalent block diagram is also shown.

where

- $\delta\nu$ is the free running laser frequency noise;
- C is the transfer function describing the photodiode response, the modulation/demodulation process, and the cavity optical response;
- H is the electronic transfer function;
- P is the efficiency of the PZT driver;
- e is the error signal, whose relationship to the free running laser frequency noise $\delta\nu$ is

$$\frac{e}{\delta\nu} = \frac{C}{1 + C \times H \times P}$$

- and y is the control signal, whose relationship to the frequency noise is

$$\frac{y}{\delta\nu} = \frac{C \times H}{1 + C \times H \times P}$$

By measuring the

1. open loop transfer function C*H*P;
2. the electronic transfer function H

3. and the DC efficiency of the PZT driver

we were able to infer, by comparing an analytical model with the measurements, the frequency dependence of C and P. Setting the electronic transfer function H to

$$H = 50 \times \frac{\omega_1}{s + \omega_1} \left[\frac{V}{V}\right]$$

we found good agreement between the data and the model if

$$C = 40 \times \frac{\omega_{rc}}{s + \omega_{rc}} \left[\frac{V}{MHz}\right]$$

where $\omega_{rc}=2*p*f_{rc}$ and f_{rc} = 37 kHz is the cavity pole and if

$$P = 0.7 \times \frac{\omega_{pzt}}{s + \omega_{pzt}} \left[\frac{MHz}{V}\right]$$

where $\omega_{pzt}=2*p*f_{pzt}$ and f_{pzt} = 90 kHz. The system here described gives an open loop DC gain of 1.4*10^3 with a unity gain frequency of 1 kHz.

By taking the spectral density of the error signal and by multiplying it by the filtering of the system, we estimated the free running laser frequency noise, shown in figure(3), to be

- $\delta\nu$ = 2kHz/rHz @ 100 Hz
- $\delta\nu$ = 30 Hz/rHz @ 1kHz
- $\delta\nu$ = 2 Hz/rHz @ 10kHz

We found this noise to be ~10 times higher than the laser specifications at 100 Hz.

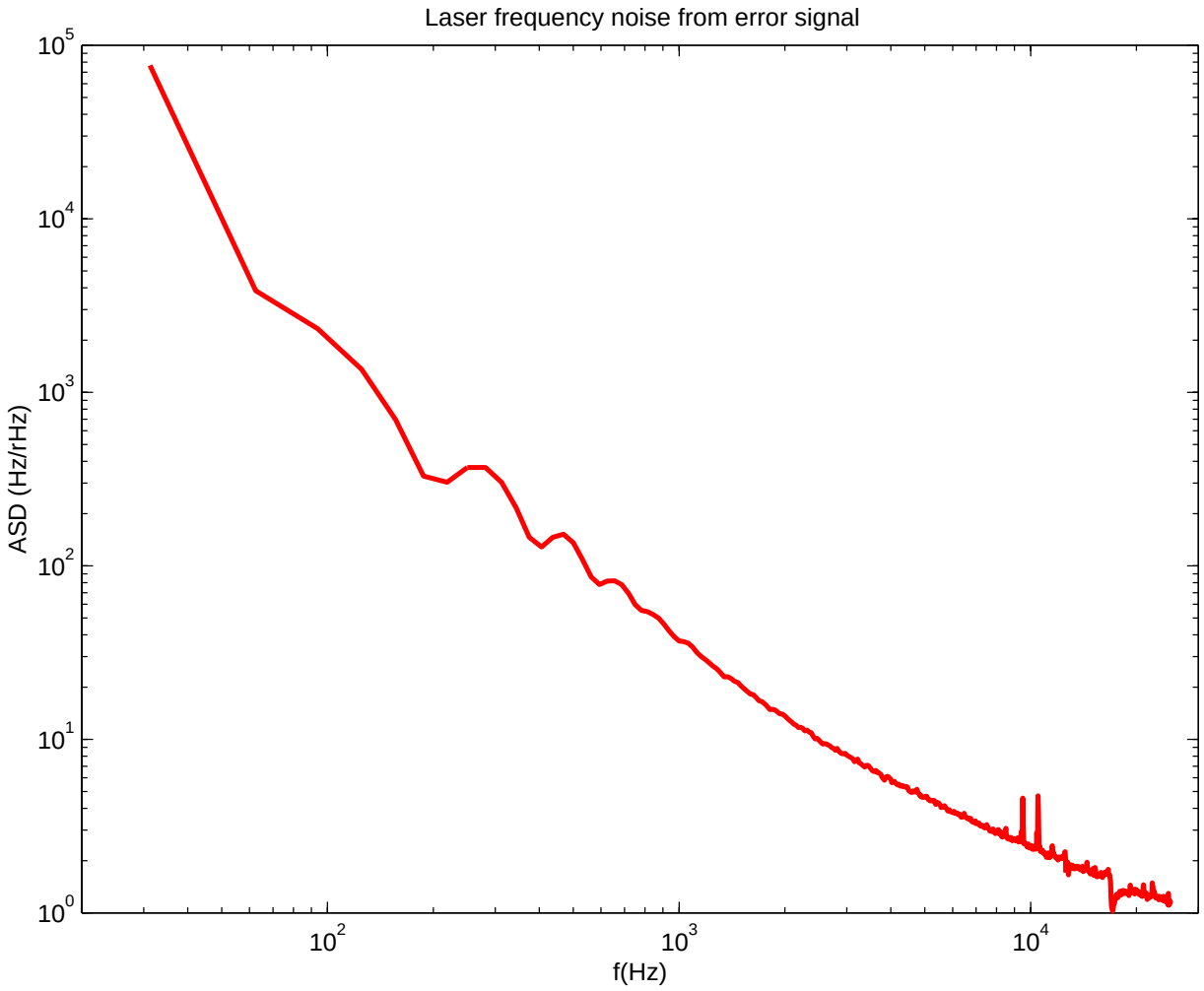

Figure 3: The free running laser frequency noise estimated from the error signal. This gives a noise of 2 kHz/rHz @ 100 Hz, 30 Hz/rHz @ 1 kHz and 2 Hz/rHz @ 10 kHz.

4 THE SUSPENDED TEST CAVITY

This section addresses the measurements completed on the system consisting of the laser and one of the suspended test cavities. The setup is represented in figure 4 together with its block diagram equivalent.

4.1. The control topology

The suspended cavity was locked by adjusting the laser frequency with the laser's PZT driver and by acting directly on the mirror through the OSEM controller. In the low frequency regime, the cavity length was modified so as to track the laser frequency whereas in the high frequency regime, the laser frequency was adjusted so as to follow the cavity resonance. Different crossover and unity gain frequencies were tested, ranging from ~40 Hz to ~800 Hz for the former and ~1kHz to ~20kHz for the latter. For the purpose of the investigations, we settled on a control topology with an overall DC gain of 2*10^6, a unity gain frequency of ~12.4 kHz and a crossover frequency of ~ 200 Hz. This configuration was robust and stable with a phase and gain margin of 20 deg and 13dB respectively and with negligible acquisition times.

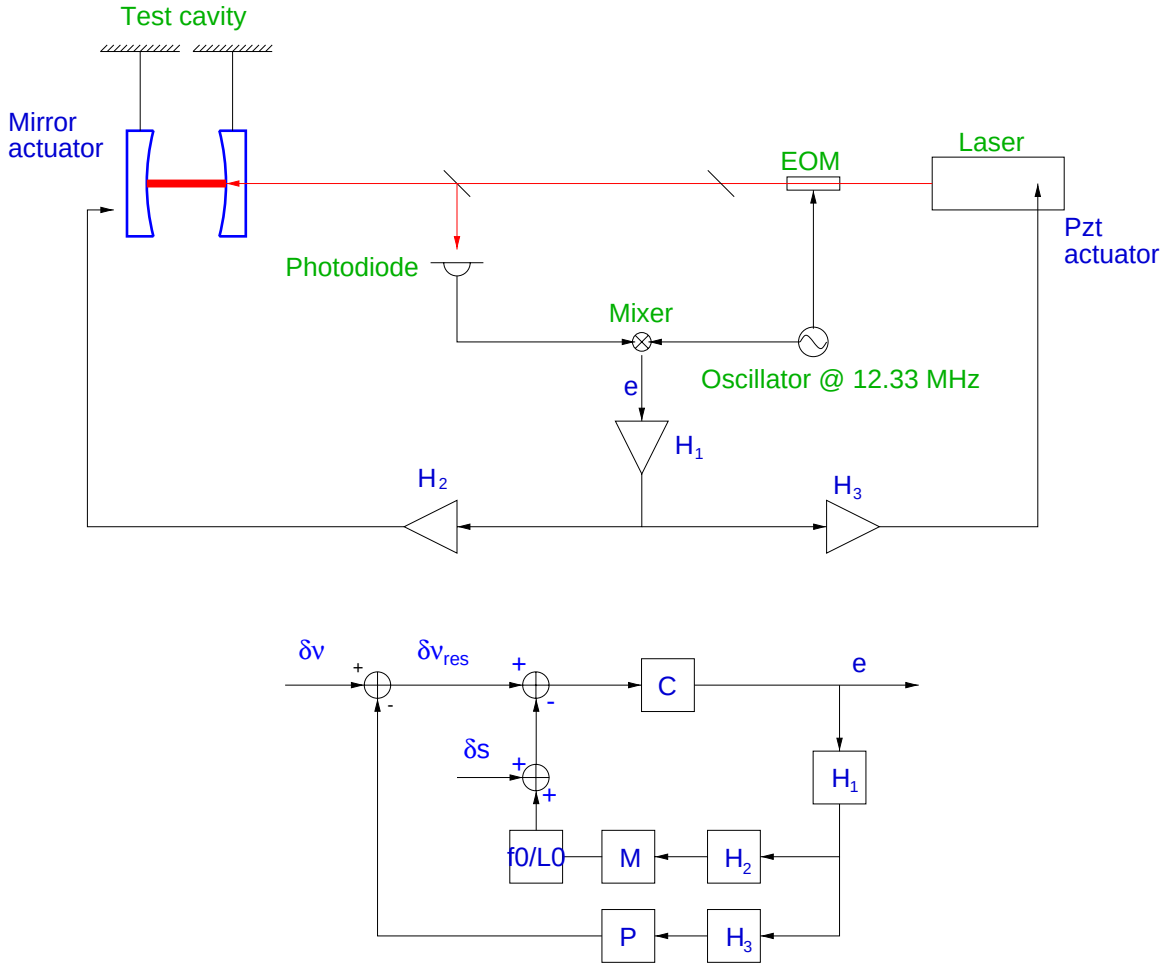

Figure 4: The test cavity control topology. The equivalent block diagram is also shown.

4.1.1. The electronic transfer functions H_1, H_2 and H_3

By following the notation of figure 4, the electronic transfer functions consisted of

- H_1 for the common path filtering, where

$$H_1 = \left(\frac{\omega_1}{s+\omega_1}\right)\left[\frac{V}{V}\right]$$

  and $\omega_1=2*p*f_1$ and $f_1=3$ kHz (in acquisition mode, $f_1=10$kHz);
- H_2 for the test cavity path filtering, where

$$H_2 = 20\times\left(\frac{\omega_2}{s+\omega_2}\right)^2\left[\frac{V}{V}\right]$$

  and $\omega_2=2*p*f_2$ and $f_2=300$ Hz;
- H_3 for the laser path filtering, where

$$H_3 = 500\times\left(\frac{\omega_3}{s+\omega_3}\right)\left[\frac{V}{V}\right]$$

  and $\omega_3=2*p*f_3$ and $f_3=10$ Hz;

4.1.2. The mirror actuator M

The frequency dependence of the mirror actuator was extracted by sending a signal to the coil drivers (a force along the beam axis) and observing the mirror motion (along the beam axis) through the optical sensor head monitors. In the frequency region below 20 Hz, the measured transfer function is shown in blue in figure 5. Two pendulum resonances are clearly visible around 1 Hz (attributed to the longitudinal (along the beam axis) and yaw modes), as well as the 1/f^2 behavior in the higher frequency region. The red curve in figure 5 corresponds to the transfer function of an harmonic oscillator of quality factor $Q_m=6$ and resonant frequency $f_m=\omega_m/(2*\pi)=1$ Hz:

$$M = G_m\times\frac{\omega_m^2}{s^2+\frac{\omega_m}{Q_m}\times s+\omega_m^2}$$

The quality factor Q_m depends on the amplitude of the excitation and for this measurement a 5 V_p signal was being sent to the actuator. Here, G_m gives the ratio between the voltage reading of the OSEM and the voltage sent to the coil driver and it is found to be

$$G_m = 54 \cdot \frac{mV}{V}$$

The purpose of this measurement was to verify the actuator's frequency response.

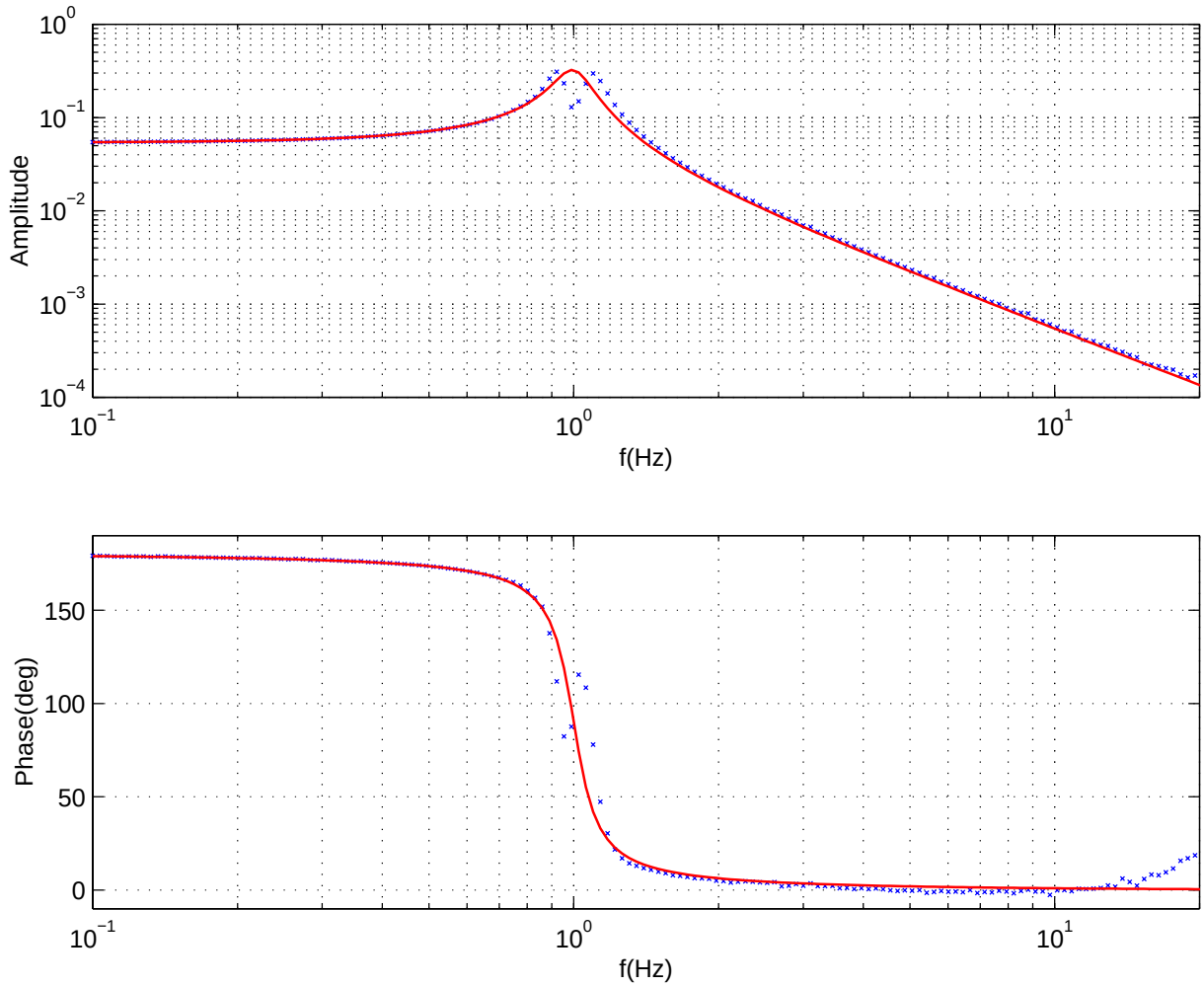

Figure 5: The mirror actuator transfer function. This was measured by monitoring the output of the optical sensor head (the signal along the cavity axis) when injecting a signal to the coils. In this measurement, the mirror was locally damped. On the same graph, we plot the transfer function of an harmonic oscillator of Q=6 and a 1 Hz resonant frequency.

4.1.3. The PZT transfer function P

The efficiency of the laser PZT driver has been discussed in section 3.

4.2. The open loop transfer function

In order to complete the characterization of the system, we needed to quantify

1. the transfer function C describing the photodiode response, the modulation/demodulation process, and the cavity optical response;
2. and the calibration factor G_m relating the displacement of the mirror to the input voltage of the OSEM.

By factoring out the known transfer functions from the measurement of the open loop transfer function, we were able to estimate C and G_m by comparing the data to an analytical model.

The measurement of the open loop transfer function was achieved by summing a test signal to the error signal. The ratio of the signal right before the summing point and right after it delivers a direct measurement of the transfer function in question (see Appendix 1 of [1]).

The red points of the graph shown in figure 6 represent the open loop transfer function measurement for the control topology, where the gain of H_2 is set to 100 instead of 20 in order to easily identify the crossover point. A qualitative agreement was achieved by setting

$$G_m = 1\left[\frac{\mu m}{V}\right]$$

and

$$C = G_c \times \frac{\omega_{tc}}{s + \omega_{tc}}\left[\frac{V}{MHz}\right]$$

where G_c=3 and by assuming that w_{tc}=2*p*120kHz is the cavity pole. The blue line in figure 6 represents the open loop transfer function from the model.

The procedure to fit the model to the measurement consisted in adjusting

1. G_c for an agreement in the high frequency domain;
2. G_m for an agreement of the crossover frequency.

We also measured G_c directly by letting the mirrors swing through a resonance, recording the error signal, and measuring its slope on an oscilloscope (we used the sidebands for calibrating the horizontal axis in units of frequency.) This procedure routinely gave G_c=20 V/MHz, which is nearly a factor of ten larger than the fit value and inconsistent with the observed unity gain frequency. We have not yet resolved this discrepancy.

Figure 6 clearly shows that the crossover point was not optimized, however this setup served well in estimating the calibration factor G_m. By replacing H_2 with its original configuration, the crossover of the two paths is improved.

The reader may also notice the disagreement between the model and the data in the low frequency region. For frequencies below 60 Hz, the overall gain is too high for a SNR>1 thus making it difficult to measure correctly the transfer function.

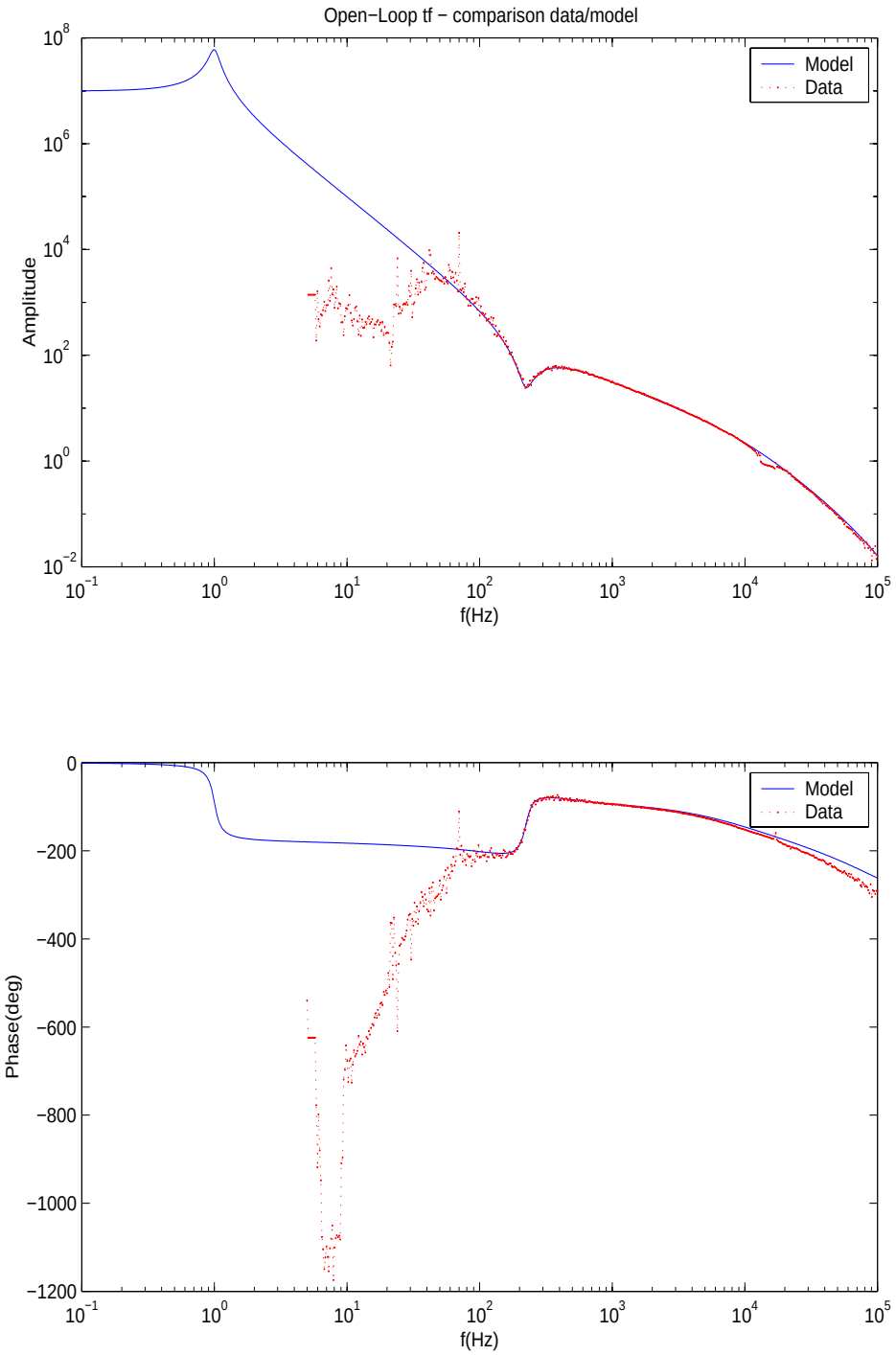

Figure 6: The open-loop transfer function of the control topology with the gain of H_2 set to 100 and comparison between the measurement and the model. For frequencies below 60 Hz, the overall gain is too high for a SNR>1.

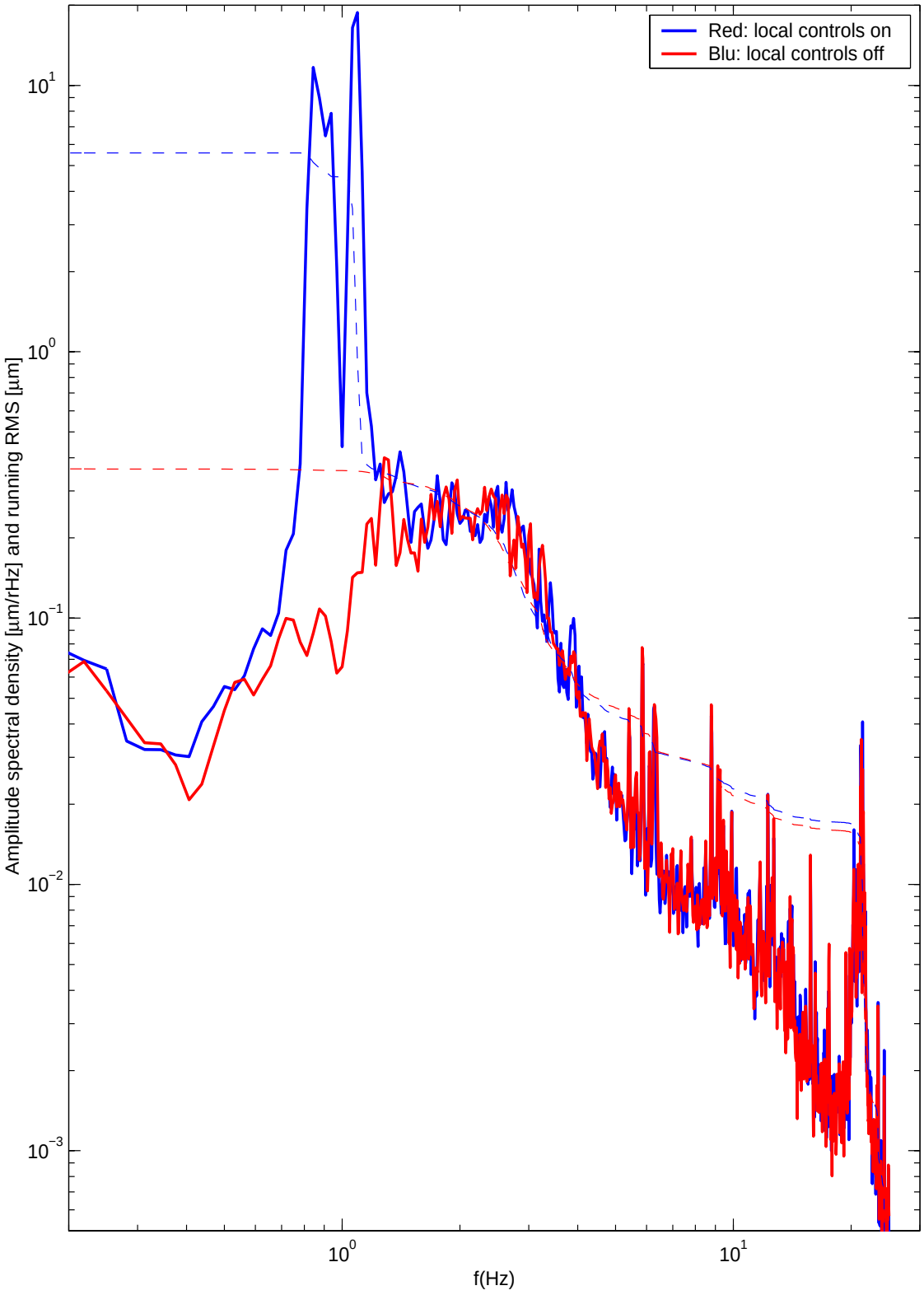

Figure 7: The estimated back mirror motion as read from the OSEM.

4.3. Performance of local controls and estimated seismic noise

Figure 7 shows the estimated displacement noise, in terms of amplitude spectral noise and running RMS, of the back mirrors as seen from the OSEM. In blue, the local control for all degrees of freedom is disabled whereas in red the local damping is enabled on all degrees of freedom.

This results in 5.6 µm RMS integrated to 200mHz when the local damping is off (free mirror) and 0.4 µm RMS also integrated to 200mHz when the local controls are enabled. The value found for the free mirror is a lower limit: this sampling does not allow to determine the Q of the resonances around 1 Hz.

Figure 7 also gives an indication of the performance of the local controls: the high Q of the resonances visible around 1 Hz are successfully lowered as the mirror is damped.

Another feature of the amplitude spectrum is the resonance located at ~21Hz. This resonance is also visible in the control signals used to keep the system on resonance and may be probably attributed to one of the stack's resonances.

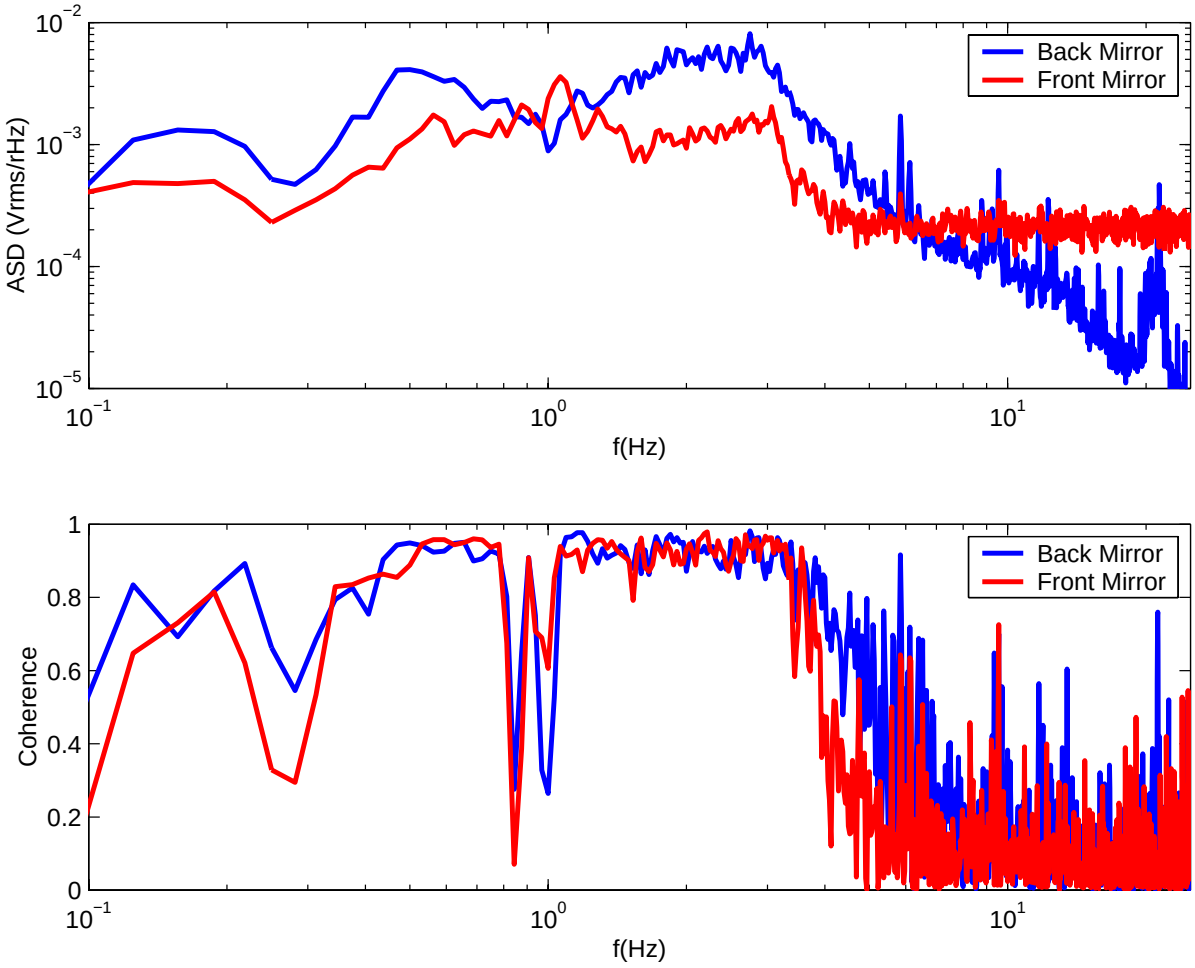

Figure 8: The amplitude spectral density of both mirrors, as read by the OSEM. The coherence between the two measurements is also shown.

Figure 8 shows the spectral density of the motion of both mirrors, again given by the OSEM, as well as the coherence of the two signals. The OSEM reading from the front mirror is dominated by noise for frequencies above 4 Hz, a factor ~20 greater than the 10^-5 V/rHz noise floor for the back mirror. Below 4 Hz, the motion of one mirror is highly correlated with the other.

5 DETECTOR SENSITIVITY

Once the interferometer, consisting of the laser source and the suspended cavity, was characterized, we estimated its displacement sensitivity and we verified that it was limited by the laser frequency noise. The spectral density of the sensitivity is shown by the blue curve in figure 9 and it was derived by filtering out the control transfer function from the spectral density of the error signal e.

Two noise sources have been plotted with the sensitivity. The green curve indicates the detector noise, which includes the photodiode and mixer noise sources. The limiting noise source, shown by the red curve, is the laser frequency noise measured with the reference cavity and discussed in section 3.The resulting displacement sensitivity is

$$\tilde{\delta s} = 2\times 10^{-15} \cdot \left[\frac{m}{\sqrt{Hz}} \right] \qquad at \qquad 1kHz$$

6 CONCLUSION

The TNI performance and characterization has been addressed and here reported. The investigation first focused on the laser/reference cavity system, resulting in the determination of the laser PZT efficiency (a factor of 6 lower than the expected value) and the free running laser frequency noise (a factor of 10 greater than the expected value at 100 Hz).

The laser/test cavity system was then explored: the performance of the mirror local damping was measured, as well as the mirror actuator. Different control topologies were tested, with and without the home made electronics designed for the operation of the Mode Cleaner, and the instrument's sensitivity was given, reaching the 10^-15 m/rHz level at 1kHz. We were able to confirm that the laser frequency noise, determined with the reference cavity, limits the displacement sensitivity.

APPENDIX 1 REFERENCE

[1] LIGO-T000077-00-R "TNI Mode Cleaner/ Laser Frequency Stabilization System"

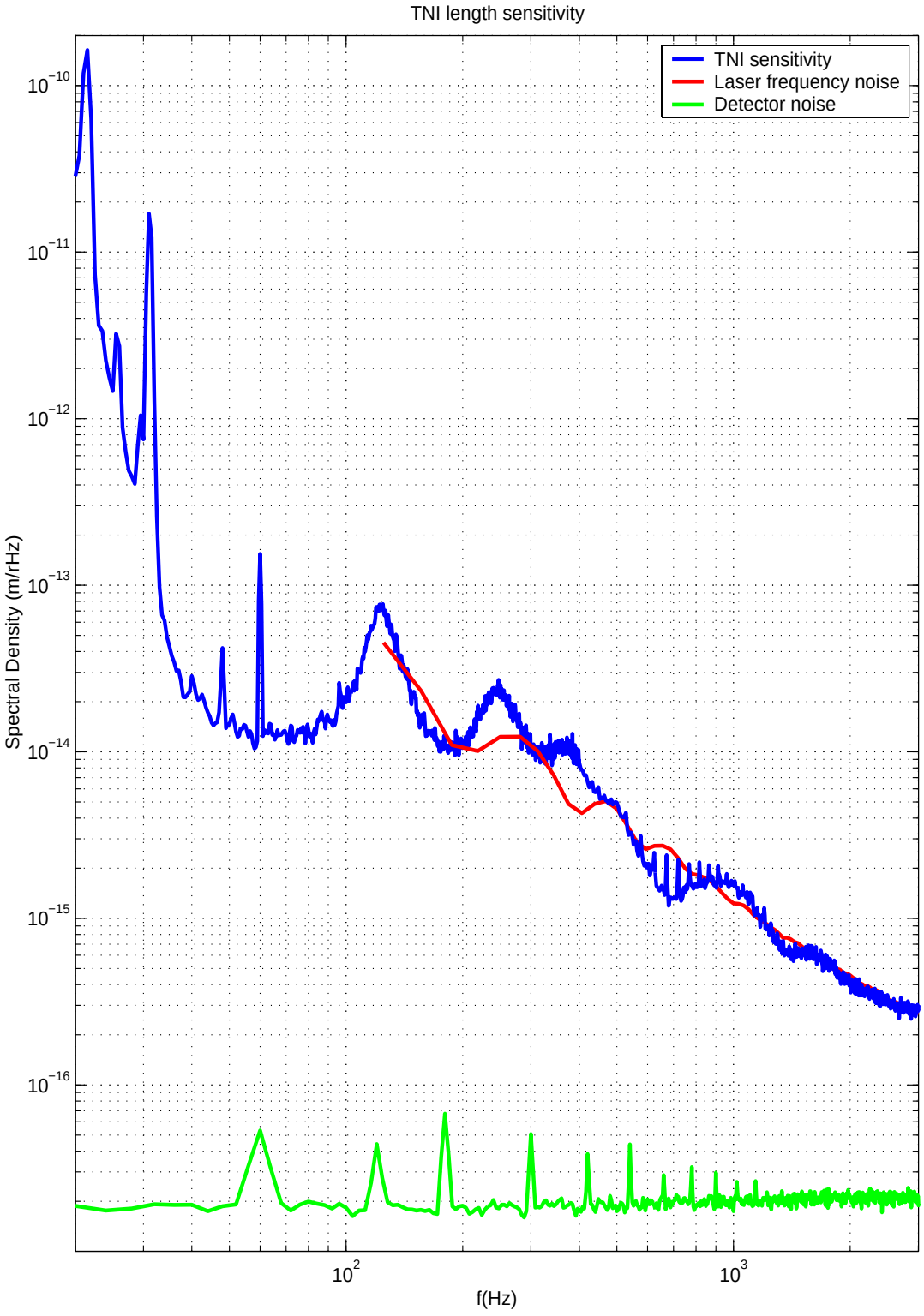

Figure 9: The instrument's displacement sensitivity and the contribution of some noise sources. In blue: the instrument sensitivity; in red: the laser frequency noise; in green: the detector noise level, including the photodiode and mixer noise sources.